RESEARCH ARTICLE

Preparation and properties of SA-BC-CS-nHAP double-layer composite biofilm

Chunliu Lv*

Department of Pharmaceutical Engineering, Hebei Chemical & Pharmaceutical College, Shijiazhuang, Hebei, China.

Received: December 11, 2025; **accepted:** April 28, 2026.

Biofilms exhibit strong antimicrobial resistance in the treatment of related infections. Traditional biofilm preparation methods suffer from environmental pollution, complex functional connections, and a lack of sufficient mechanical and biocompatibility under physiological conditions. This study prepared a double-layer composite biofilm with excellent mechanical stability, good cell compatibility, and highly efficient antimicrobial properties. Sodium alginate meeting the requisite standards and bacterial cellulose produced by *Acetobacter xylinum* were selected to prepare a bilayer composite biofilm consisting of sodium alginate, bacterial cellulose, chitosan, and nano-hydroxyapatite (SA-BC-CS-nHAP) using a stepwise gradient cross-linking method. Subsequently, the structure of the composite was characterized, and its mechanical and biological properties were evaluated. The results showed that, when the mass ratio of sodium alginate to bacterial cellulose was 10:1, the dry tensile strength of the composite biofilm reached 15.3 MPa, the wet tensile strength was 8.2 MPa, and the 28-day mass loss rate was only 7.3%. The relative proliferation rate in the low-concentration extract solution was 85%, and the 24 h OD values against *Staphylococcus aureus* and *Escherichia coli* were 0.32 and 0.35, respectively. The double-layer composite biofilm demonstrated excellent performance and provided a feasible solution for developing biofilm materials related to the biomedical field, especially oral or tissue repairing.

Keywords: composite biofilm; gradient cross-linking method; mechanical stability; cytocompatibility; antibacterial properties.

***Corresponding author:** Chunliu Lv, Department of Pharmaceutical Engineering, Hebei Chemical & Pharmaceutical College, Shijiazhuang, Hebei 050030, China. Email: lcl@hebcpc.edu.cn.

Introduction

Biofilms are complex community structures formed by microbial aggregation, widely present in various fields such as medicine, food, and water treatment. Their core hazard lies in the protective effect of extracellular polymeric matrices, which not only can isolate external intervention substances like antibiotics and fungicides, significantly enhancing bacterial resistance, but also exacerbate the persistence and non-healing of infections, increasing treatment costs and patient burdens [1, 2]. In recent years, nanotechnology has provided a new perspective for regulating biofilms, and related research has achieved many advancements.

Brezhnev *et al*. used a one-pot method to load disinfectant drug hexadecyl chloropropyl pyridine and developed a preparation method for a biofilm-targeted delivery system that could prolong the drug release time, effectively killed the tested bacteria in the biofilm to address the

dental caries and pulp lesions caused by oral infection-related bacteria. The particle size could penetrate the dentin tubules, having potential applications in the dental material field [3]. To address the environmental non-compatibility of organic solvents in traditional biofilm preparation, functional component extraction and film-forming process connection in complex issues, Mussagy *et al*. proposed a preparation method using choline low-melting-point solvents as a substitute solvent, which was simple to operate and environmentally friendly, and the resulting rich carotenoid functionalized biofilm had promising prospects [4]. Hu *et al*. designed a multifunctional self-driven micro-robot method to solve the problem that bacterial biofilms were difficult to clear by antibiotics and fungicides due to the protection of extracellular matrix. After integrating antibacterial peptides, the micro-robot could autonomously move towards bacterial cells and mechanically enter the biofilm. This micro-robot could effectively clear the biofilm and could be extended for drug delivery, having significant application potential in the field of biomedicine [5]. Asare *et al*. addressed the strong antibacterial resistance caused by extracellular polymer matrices in biofilm-related infections, combining nanotechnology with traditional antibacterial treatment methods. Various strategies for biofilm prevention and clearance were developed such as enzyme-functionalized antibacterial nanocarriers and biofilm microenvironment-responsive preparations, achieving targeted effects at the infection site, degradation of extracellular polymer matrices, and efficient antibacterial performance [6]. However, there are still many problems to be solved in the current research on biofilm related materials. Traditional biofilm material preparation processes have long relied on organic solvents, which not only cause environmental burdens but also may leave harmful substances that affect biological safety. Moreover, the connection between functional component extraction and film-forming preparation process is poor, not only reducing the preparation efficiency but also easily causing the inactivation of functional components [7, 8]. Existing nanocapsule-based solutions mostly focus on optimizing a single function, ignoring the core requirements of materials in the physiological environment. Some nanocapsules have excellent antibacterial effects but weak mechanical properties that cannot withstand the dynamic stress during tissue repair, and some degradable membrane materials have good biocompatibility but are prone to swelling and quality loss after long-term immersion, making it difficult to maintain stable structure and function [9, 10].

This research constructed a composite biofilm with structurally adapted, performance-coordinated, and safe application, addressing the insufficient mechanical stability, cell compatibility, and antibacterial performance synergy of existing materials, and meeting the comprehensive performance requirements of materials in the field of biomedicine. Biocompatible sodium alginate (SA), bacterial cellulose (BC) produced by *Acetobacter*, highly deacetylated chitosan with antibacterial activity (CS), and nano hydroxyapatite (nHAP) were used in this research. The double-layer composite structure was designed by using a stepwise gradient cross-linking method that strengthened the interface bonding of the materials and eliminated the traditional organic solvent process, optimizing the connection process between functional components and film-forming preparation to simultaneously enhance the mechanical stability, cell compatibility, and efficient antibacterial function of the materials in the physiological environment. This research overcame the industry challenge of the difficulty in balancing the mechanical properties and biological functions of materials in a single structure by combining a double-layer composite structure with a gradient cross-linking method. The resulting SA-BC-CS-nHAP double-layer composite biological membrane possessed excellent mechanical stability, good cell compatibility, and efficient antibacterial properties, which provided a feasible solution for developing biofilm materials in the biomedical field, especially for oral or tissue repair-related

biofilm materials and filled the research gap of insufficient multi-performance synergy of existing materials and had significant scientific value and practical significance for promoting the research and clinical application of biofilm materials.

Materials and methods

Specification of experimental materials

Sodium alginate (SA) (Shanghai Maclin Biochemical Technology Co., Ltd., Shanghai, China) was a high-purity, linear anionic polysaccharide, preferably extracted from brown algae. Its viscosity was controlled within the range of 0.025 to 0.030 Pa·s to ensure uniform dispersion when mixing with bacterial cellulose (BC) and facilitate the formation of a structurally dense, layered architecture following evaporation-induced self-assembly, while simultaneously enhancing the film's resistance to swelling after cross-linking with calcium ions. Biochemical grade BC (Nanjing Tianlu Nanotechnology Co., Ltd., Nanjing, Jiangsu, China) was selected and prepared by *Acetobacter xylin* fermentation [11, 12]. The fiber diameter was controlled at 20 – 50 nm and the crystallinity was ≥ 90%. High crystallinity could give the composite biofilm excellent mechanical support ability. Its three-dimensional network structure could form hydrogen bonds with SA to further enhance the tensile strength of the film. Medium and low viscosity chitosan (CS) (Jiangsu Kangting Biotechnology Co., Ltd., Yancheng, Jiangsu, China) with deacetylation degree of ≥ 95% and high deacetylation was selected for this study. The acidity ensured that it was fully dissolved in the acidic solution and could form an electrostatic interaction with the anionic group of SA through the cationic properties, improving the interfacial bonding force of the double-layer film and exerting antibacterial activity simultaneously. Nano hydroxyapatite (nHAP) powder (Wuhan Pushida Biotechnology Co., Ltd., Wuhan, Hubei, China) was used with a particle size of 50 – 100 nm and crystal structure ≥ 95% similar to the inorganic components of human bone matrix to avoid uneven functional activity caused by agglomeration [13, 14]. Phosphate buffer saline (PBS) with pH of 7.2 - 7.4 was employed to simulate the human body fluid environment.

Preparation of SA-BC-CS-nHAP double-layer composite biofilm

The study employed the stepwise gradient cross-linking method to prepare the SA-BC-CS-nHAP double-layer composite biological membrane. By adjusting the formation parameters of the underlying dense layer and the upper porous layer combined with the interface cooperative cross-linking technology, the double-layer bonding force was enhanced [15, 16]. The underlying SA-BC dense membrane was prepared by the ultrasonic assisted blending - vacuum evaporation film forming process. Briefly, BC was dispersed in deionized water and treated with 1,000 W power ultrasonic treatment for 30 minutes to prepare a uniform BC suspension with a concentration of 0.5%. High purity SA powder was then added to the BC suspension in the ratios SA to BC as 8:1, 10:1, and 12:1, respectively. The mixture was stirred at 600 rpm for 2 h until complete dissolution to form an SA-BC mixture before being poured into a polytetrafluoroethylene mold and placed in DHG-9240A constant temperature drying oven (Shanghai Yiheng, Shanghai, China) at -0.09 MPa. The surface moisture was evaporated at 30℃ for 4 h followed by drying at 45℃ for 12 h to obtain a pre-formed SA-BC membrane with a thickness of approximately 80 μm. The pre-formed membrane was immersed in a 2% (w/v) calcium chloride - anhydrous ethanol solution for cross-linking at 25℃ for 60 minutes before being rinsed with deionized water for 3 times to remove residual calcium ions. After vacuum drying, a dense underlying layer membrane was obtained. The upper CS-nHAP porous layer was prepared by the electrospinning – freeze drying process. CS was dissolved in 1% (v/v) glacial acetic acid solution and mixed for 4 hours to prepare a 4% CS solution. nHAP powder was then added at the ratios of nHAP to CS at 1:5, 1:10, and 1:15, respectively. After 20 minutes of ultrasonic

dispersion at 800 W power, 0.5% (w/v) polyvinylpyrrolidone (PVP) K30 was added as a spinning aid, and the mixture was stirred evenly to obtain the CS-nHAP spinning solution that was then spun at 25℃ with a spinning rate of 0.8 mL/h, a relative humidity of 40 - 45%, onto the surface of the underlying SA-BC dense membrane with a spinning time of 30 - 60 minutes to form a fiber precursor layer with a thickness of approximately 150 - 200 μm. The composite membrane with the loaded fiber layer was transferred to -80℃ for pre-freezing for 2 h before freeze drying for 24 h to form a connected porous structure between the fibers by using FD-1C-80 freeze drying machine (Beijing Songyuan Huaxing, Beijing, China). The interface of the double-layer membrane was strengthened through alkaline treatment and secondary cross-linking. The freeze-dried composite membrane was immersed in a 0.1 mol/L sodium hydroxide solution at 30°C for 30 minutes. Partial de-acetylation of the CS fiber layer was achieved through alkali diffusion, allowing the dissociated negatively charged -COO^- in the SA molecules to interact with the positively charged -NH^{3+} formed by protonation in the CS molecules through positive and negative charge attraction, thereby enabling a close binding between SA and CS. After removal, it was immediately transferred to a 0.05 mol/L calcium chloride solution at 20°C for secondary cross-linking for 40 minutes. The Ca^{2+} ions diffused to the interface region, forming ionic bonds with the -COO^- of SA and interacting with the hydroxyl groups -OH of CS, further strengthening the ionic bonding between SA and CS, and achieving the interface cross-linking stability of the double-layer composite biological membrane. In the post-treatment stage, the composite membrane was ultrasonically cleaned in deionized water to remove residual reagents and then dried in a vacuum drying box at 37°C for 8 hours. A SA-BC-CS-nHAP double-layer composite biological membrane with a thickness of approximately 250 - 300 μm was eventually obtained.

Characterization and performance evaluation of SA-BC-CS-nHAP double-layer composite biofilm

The microscopic morphology of the SA-BC-CS-nHAP double-layer composite biofilm was obtained by using scanning electron microscopy (SEM). The dense layer structure of the underlying SA-BC, the pore structure of the porous layer of CS-nHAP, and the dispersion of nHAP particles were observed. The phase composition of the material was analyzed by using X-ray diffraction (XRD) to verify the retention of the nHAP crystal structure and the composite effect of each component. The chemical structure of the material was analyzed by Fourier transform infrared spectrometer (FTIR) to confirm the integration of the characteristic absorption peaks of each individual component and the formation of the composite system [17, 18]. *In vitro* biological performance of the SA-BC-CS-nHAP double-layer composite biofilm was evaluated by using the MTT colorimetric method. Mouse fibroblast cells (L929) were cultured in α-MEM medium (Gibco, Grand Island, NY, USA) containing 10% fetal bovine serum (FBS) and 1% double antibiotics of 100 U/mL penicillin and 100 μg/mL streptomycin at 37°C and 5% CO_2. After the cells were seeded in 96-well plates, different concentrations of 0.1, 1, 10, and 100 mg/mL of the extract from the composite membrane were added with medium only as blank control and cell culture without the extract as negative control. After 24 h, 48 h, and 72 h of culture, MTT reagent (Sigma-Aldrich, St. Louis, MO, USA) was added for incubation for 4 h. After discarding supernatant, dimethyl sulfoxide (DMSO) was added to dissolve the crystals. The absorbance at 490 nm was measured by using a plate reader (Thermo Fisher Scientific, Waltham, MA, USA). The cell viability was calculated to evaluate the cell compatibility and cytotoxicity of the material. The antibacterial performance of the SA-BC-CS-nHAP double-layer composite biofilm was evaluated by using the inhibition zone method and bacterial viable count method. *Staphylococcus aureus* (ATCC 25923) and *Escherichia coli* (ATCC 25922) were employed. The bacteria were resuscitated in nutrient broth medium and cultured in a shaking incubator at 37°C until the logarithmic growth phase. The bacterial solution concentration was

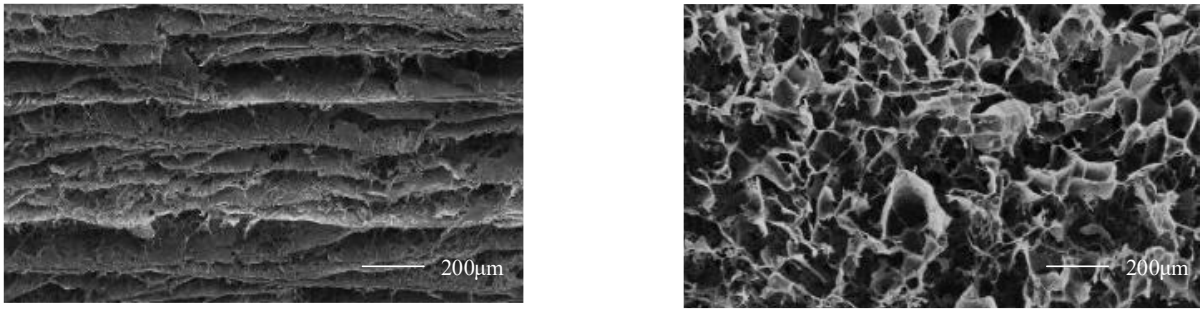

(a) SA-BC dense layer (b) CS-nHAP porous layer

Figure 1. SEM of SA-BC-CS-nHAP double-layer composite biofilm.

adjusted to approximately 10^8 CFU/mL. The SA-BC-CS-nHAP composite membrane, pure SA membrane, pure BC membrane, pure CS membrane, and pure nHAP membrane were respectively placed on agar plates coated with bacterial solutions. After 24 h of incubation at 37°C, the diameter of the inhibition zone was measured. After co-incubating the composite membrane with the bacterial solution for 0.5, 1, 2, and 4 h, the supernatant was gradient diluted and plated on the plate for bacterial viable counting. The viable count and antibacterial rate were then calculated. To evaluate the mechanical stability of the SA-BC-CS-nHAP double-layer composite biofilm, polyacrylate films, carboxymethyl cellulose films, hydroxyapatite/gelatin films (nHAP/Gel), collagen films (Col), and polylactic acid films (PLA) were selected as control samples. All the film samples were cut to standard sizes and immersed in simulated body fluid for 24 h before the wet tensile strength, elongation at break, and elastic modulus being tested following the ASTM D882 standard. The force-displacement data were recorded, and the mechanical parameters were calculated. All tests were conducted at room temperature with 3 parallel samples from each group to ensure data reliability.

Statistical analysis

The experimental data were statistically analyzed by using SPSS Statistics 26.0 software (IBM, Armonk, NY, USA). The data were expressed as mean ± standard deviation. The inter-group comparison was conducted by using one-way analysis of variance (ANOVA), and pairwise comparisons were performed by using the LSD method. *P* value less than 0.05 was considered statistically significant.

Results and discussion

Microstructure and composition characterization of SA-BC-CS-nHAP double-layer composite biofilm

The SEM results of SA-BC-CS-nHAP double-layer composite biofilm showed that the SA-BC dense layer presented a continuous layered structure without obvious pores. The layers were tightly stacked. The BC nanofibers interwove with the SA matrix to form a uniform dense base, which provided good mechanical support and barrier function for the film (Figure 1a). The CS-nHAP porous layer exhibited a richly connected pore structure with uniform pore distribution. CS fibers were interwoven into a network skeleton, and nHAP particles were evenly dispersed on the fiber surface and in the gaps. This porous structure was conducive to cell adhesion, migration, and nutrient exchange (Figure 1b). The XRD of SA-BC-CS-nHAP double-layer composite biofilm demonstrated that nHAP had a characteristic diffraction peak at about 50° in 2θ, which had obvious crystal structure characteristics. The diffraction peaks of SA, BC, and CS were relatively gentle, showing typical amorphous or weak crystalline characteristics.

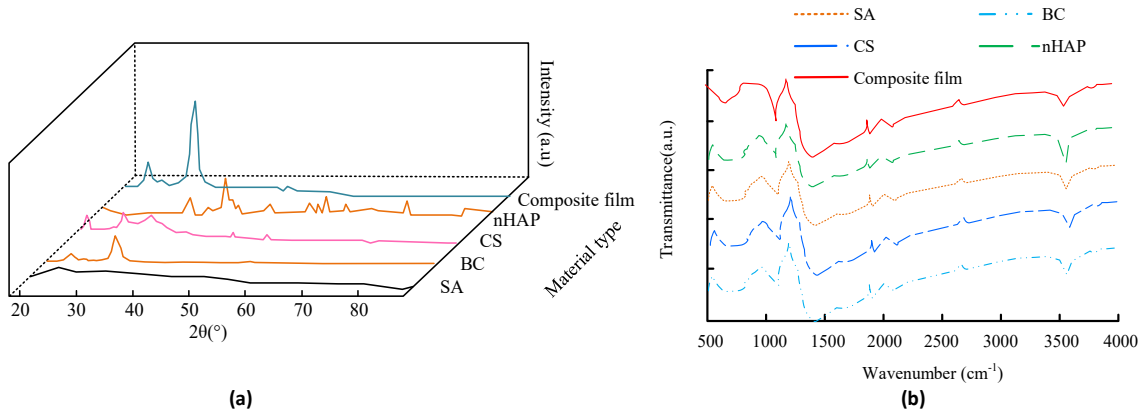

Figure 2. XRD (**a**) and FTIR (**b**) of SA-BC-CS-nHAP double-layer composite biofilm.

Table 1. Dry mechanical properties of composite biofilm at different SA-BC mass ratios.

Serial number	SA-BC mass ratio	Dry tensile strength (MPa)	Standard deviation (MPa)	Elongation at break (%)	Standard deviation (%)	Mechanical property grade
1	6:1	10.2 ± 0.7	0.7	8.5 ± 0.5	0.5	III
2	8:1	12.6 ± 0.8	0.8	10.3 ± 0.6	0.6	II
3	10:1	15.3 ± 0.6	0.6	12.1 ± 0.4	0.4	I
4	12:1	9.8 ± 0.7	0.7	7.8 ± 0.5	0.5	III
5	14:1	7.5 ± 0.6	0.6	6.3 ± 0.4	0.4	IV
6	16:1	5.9 ± 0.5	0.5	4.9 ± 0.3	0.3	IV

The diffraction curve of the composite biofilm not only retained the characteristic peaks of nHAP but also integrated the diffraction information of SA, BC, and CS. This showed that, during the preparation process of the double-layer composite biofilm, the crystal structure of nHAP was not destroyed and was successfully combined with SA, BC, and CS to form a composite structure with both an inorganic crystal phase and an organic amorphous phase (Figure 2a). The FTIR of SA-BC-CS-nHAP double-layer composite biofilm showed that the infrared curve of the composite biofilm integrated the characteristic absorption peaks of each single component, and no new impurity peaks appeared. During the preparation process of the double-layer composite biofilm, physical or chemical combinations occurred between SA, BC, CS, and nHAP, successfully forming a composite system while retaining the structural characteristics of each component (Figure 2b).

Mechanical property and stability of SA-BC-CS-nHAP double-layer composite biofilm

The results showed that, when the SA-BC mass ratio increased from 6:1 to 10:1, the tensile strength increased from 10.2 MPa to 15.3 MPa with an increase of 50.0%, and the standard deviation decreased from 0.7 MPa to 0.6 MPa. BC nanofibers were evenly dispersed in the SA matrix in this interval, forming a continuous support network, and the fiber reinforcement effect was significant. After the ratio exceeded 10:1, the strength continued to decrease and dropped to 5.9 MPa at 16:1, which was 61.4% lower than that at 10:1. It was because the BC content was too low to form an effective support, and the matrix was easy to break. The change trend of elongation at break was consistent with the tensile strength, reaching the maximum value of 12.1% at 10:1, which was 146.9% higher than that at 16:1, indicating that the film material at this ratio had both high strength and good toughness (Table 1). Taken together, when the

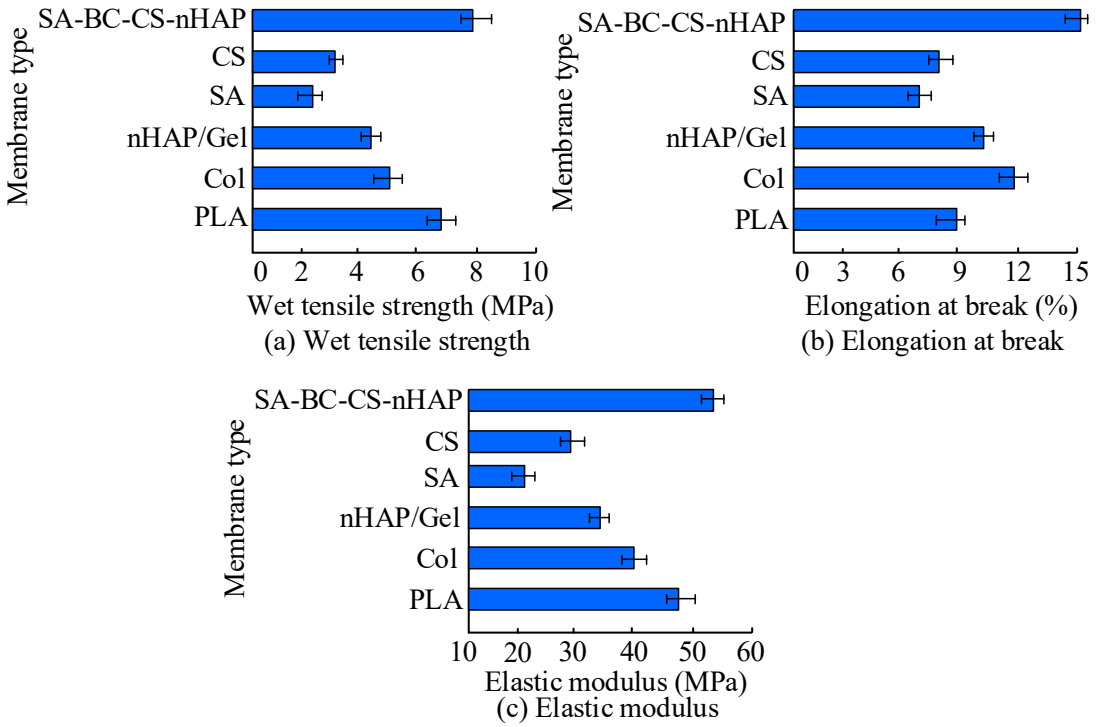

Figure 3. Wet mechanical properties of different biofilms in simulated body fluid environment.

SA-BC mass ratio was 10:1, the tensile strength and elongation at break of the composite biofilm were optimal and could provide stable mechanical support and certain deformation ability for the double-layer biofilm structure. Further, the wet tensile strength of the SA-BC-CS-nHAP double-layer composite biofilm reached 8.2 MPa, which was higher than that of the CS film (3.1 MPa), the SA film (2.5 MPa), the nHAP/Gel film (4.6 MPa), the Col film (5.3 MPa), and the PLA film (6.8 MPa) (Figure 3a). The elongation at break of the SA-BC-CS-nHAP double-layer composite biofilm was 15.6%, which was significantly higher than that of the other five films with 88.0% higher than the CS film, 132.8% higher than the SA film, 52.9% higher than the nHAP/Gel film, 28.9% higher than the Col film, and 64.2% higher than the PLA film (Figure 3b). The elastic modulus of the SA-BC-CS-nHAP double-layer composite biofilm was 52.3 MPa, which was higher than that of CS film, SA film, nHAP/Gel film, and Col film, and had advantages compared with PLA film's 48.2 MPa (Figure 3c). The results suggested that the SA-BC-CS-nHAP composite biofilm had both high strength and high toughness in a simulated body fluid environment, and the synergistic effect of each component in the double-layer structure allowed it to maintain excellent mechanical stability in a physiological wet environment. The SA-BC-CS-nHAP composite biofilm performed the best on long-term stability. In terms of elongation at break, its 28-d toughness retention rate reached 75.6%, which was 4.6 times that of the SA film and 4.2 times that of the CS film. The amplitude of toughness attenuation was much lower than that of the control film (Figure 4a). In terms of mass loss rate, the total degradation amount of the SA-BC-CS-nHAP composite biofilm on the 28th day was only 7.3%, less than one-third of the SA film (23.8%), and the degradation increase (508.3%) was only 1/2 of the SA film (1,033.3%) (Figure 4b). The double-layer structure of the composite biofilm could effectively delay the erosion of the material by simulated body fluids while retaining good toughness. The long-term dynamic mechanical stability of the SA-BC-CS-nHAP composite biofilm in simulated body fluids

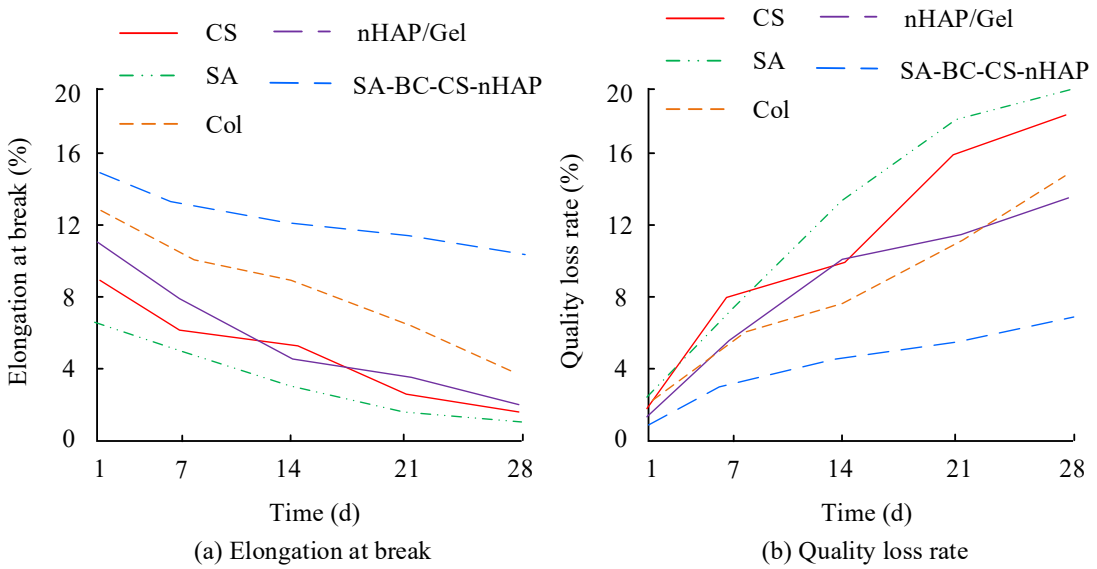

Figure 4. Comparison of elongation at break and mass loss rate of different biofilms.

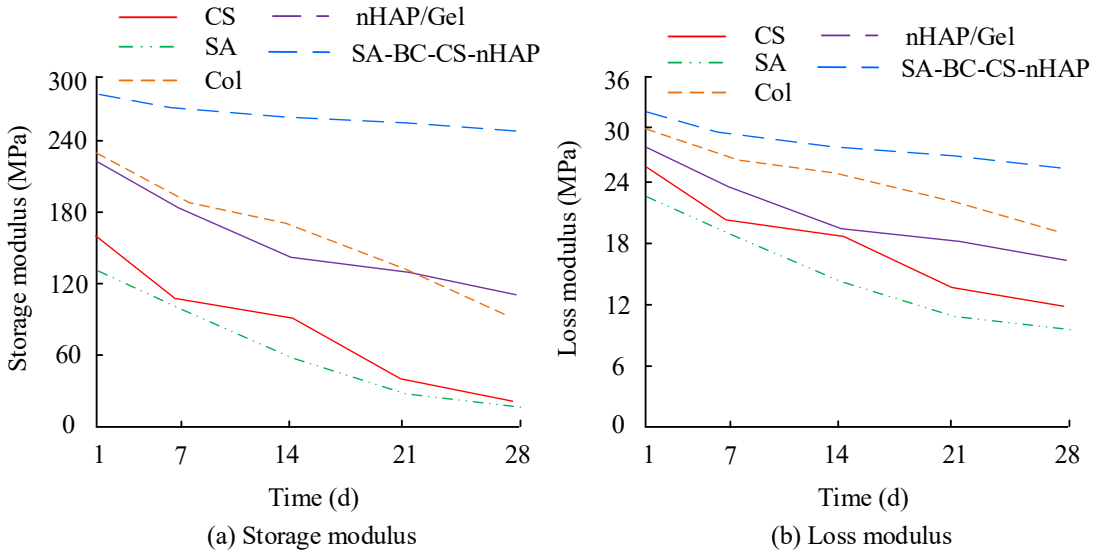

Figure 5. Comparison of long-term elastic stability and energy dissipation characteristics of different films.

was significantly better than that of the control film. In terms of storage modulus, the 28-d retention rate of the composite biofilm reached 75.4%, which was 3.0 times that of the SA film (25.0%) and 2.2 times that of the CS film (33.6%). The attenuation amplitude of the elastic deformation ability was only ½ - ⅓ of the control film (Figure 5a). In terms of loss modulus, the change range of the composite biofilm in 28 days was only -21.9%, which was lower than -59.1% of the SA film and -52.0% of the CS film, indicating that its energy dissipation characteristics were more stable and the viscoelastic balance was less affected by simulated body fluids (Figure 5b). This was due to the synergistic effect of the elastic support of the SA-BC dense layer and the energy buffering of the CS-nHAP porous layer in the double-layer structure, which maintained good dynamic mechanical properties in long-term physiological environments and adapted to

Table 2. Cytocompatibility evaluation table of composite films.

Group	Absorbance value (A)	Cell relative proliferation rate (%)	Cytotoxicity rating
Negative control group	1.00 ± 0.05	100	Grade 0 (Non-toxic
Positive control group	0.20 ± 0.03	20	Grade 4 (Strong Toxicity)
Low-concentration group of composite film extract solution	0.85 ± 0.04	85	Grade 1 (Mild toxicity)
Concentration group in the composite film extraction solution	0.75 ± 0.05	75	Grade 2 (Moderate toxicity)
High-concentration group of composite film extraction solution	0.60 ± 0.04	60	Grade 3 (Severe Toxicity)

Table 3. Comparison of antibacterial properties of *Staphylococcus aureus* and *Escherichia coli*.

Film type	Bacterial species	0 h OD value	12 h OD value	24 h OD value
SA-BC-CS-nHAP	*Staphylococcus aureus*	0.04 ± 0.01	0.20 ± 0.03	0.32 ± 0.03
	Escherichia coli	0.05 ± 0.01	0.22 ± 0.03	0.35 ± 0.03
CS	*Staphylococcus aureus*	0.04 ± 0.01	0.75 ± 0.04	1.25 ± 0.06
	Escherichia coli	0.05 ± 0.01	0.80 ± 0.04	1.32 ± 0.06
SA	*Staphylococcus aureus*	0.04 ± 0.01	0.88 ± 0.05	1.48 ± 0.07
	Escherichia coli	0.05 ± 0.01	0.95 ± 0.05	1.55 ± 0.07
Control group	*Staphylococcus aureus*	0.04 ± 0.01	0.98 ± 0.05	1.52 ± 0.07
	Escherichia coli	0.05 ± 0.01	1.05 ± 0.05	1.60 ± 0.07

dynamic stress scenarios in biomedical applications.

In vitro biological performance evaluation and statistical analysis

The results of MTT assays showed that the relative proliferation rate of cells in the low-concentration group of composite biofilm extract solution was higher, and the cytotoxicity rating was level 1, indicating that the composite biofilm was less toxic to cells at this concentration and had better cytocompatibility. As the concentration of the composite biofilm extract increased, the relative cell proliferation rate gradually decreased, and the cytotoxicity rating increased (Table 2). However, even at high concentrations, the relative cell proliferation rate still reached 60%, indicating that the composite biofilm had certain cytocompatibility and could be used for biomedical applications within a suitable concentration range. The antibacterial properties of the SA-BC-CS-nHAP composite biofilm demonstrated that the composite biofilm had a significant and sustained inhibitory effect on both bacteria. The results showed that, at 24 h, the OD value against *Staphylococcus aureus* was 0.32 with an increase of 0.28 compared with 0 h, while the OD value against *Escherichia coli* was 0.35 with an increase of 0.30 compared with 0 h. The OD values of the CS film against the two bacteria at 24 h reached 1.25 and 1.32, respectively. The OD values of the SA film and the control group increased even higher, exceeding 1.4 (Table 3). The results confirmed that the SA-BC-CS-nHAP composite biofilm had the best antibacterial effect and could effectively inhibit bacterial proliferation, which was much better than the control film. The statistical analysis results of the wet-state mechanical property data of each membrane after being immersed in simulated body fluid for 24 h showed that the wet tensile strength, elongation at break, and elastic modulus of the SA-BC-CS-nHAP composite membrane were significantly higher than those

Table 4. Statistical analysis of the wet-state mechanical properties of SA-BC-CS-nHAP composite membranes and control membranes.

Type of membrane material	Hydraulic tensile strength (MPa)	Break elongation (%)	Elastic modulus (MPa)
SA-BC-CS-nHAP composite membrane	8.2 ± 0.3	15.6 ± 0.5	52.3 ± 1.2
Polyacrylate film	5.1 ± 0.4*	8.3 ± 0.3*	35.6 ± 1.0*
Carboxymethyl cellulose film	2.8 ± 0.2*	6.5 ± 0.2*	22.4 ± 0.8*
nHAP/Gel film	4.6 ± 0.3*	10.2 ± 0.4*	38.5 ± 0.9*
Col film	5.3 ± 0.3*	12.1 ± 0.4*	41.7 ± 1.1*
PLA film	6.8 ± 0.4*	9.5 ± 0.3*	48.2 ± 1.0*

Note: * indicated $P < 0.05$ compared to the SA-BC-CS-nHAP composite membrane.

of the polyacrylic acid film, carboxymethyl cellulose film, nHAP/Gel film, Col film, and PLA film ($P < 0.05$). The wet tensile strength was 20.6% higher than that of the most performance-optimal PLA film, the elongation at break was 28.9% higher than that of the Col film, and the elastic modulus was 8.5% higher than that of the PLA film (Table 4). The results clearly indicated that the mechanical stability of the SA-BC-CS-nHAP composite membrane in the physiological environment was significantly superior to that of the control membrane materials. The double-layer composite structure and the synergistic effect of each component endowed the material with more excellent wet-state mechanical properties.

Conclusion

The SA-BC-CS-nHAP double-layer composite biofilm achieved a synergistic improvement in mechanical stability, cell compatibility, and antibacterial performance. Its double-layer structure and gradient cross-linking process effectively solved the problem that a single structural material was difficult to balance mechanical and biological functions. In the physiological environment, it exhibited superior structural stability and performance compatibility to traditional membrane materials. This composite membrane balanced efficient antibacterial and low cytotoxicity by relying on the characteristics of natural raw materials, avoiding the safety risks brought by metal ion antibacterial. It provided new technical ideas and feasible solutions for the research and development of biofilm materials in the biomedical field, especially in the field of oral and tissue repair. In future, the *in vivo* application effect of the material should be verified through animal experiments, and the release rate of antibacterial components can be optimized by combining micro-environment response design to further enhance the clinical application value of this material.

Acknowledgements

The research was supported by “Research on the Preparation Process of Zero Pollution Degradable Corn Straw Cellulose Membrane” by Hebei Chemical and Pharmaceutical Vocational and Technical College in 2025 (Grant No. YZ2025002).

References

1. Li P, Tong X, Wang T, Wang X, Zhang W, Qian L, *et al*. 2023. Biofilms in wound healing: A bibliometric and visualized study. Int Wound J. 20(2):313-327.
2. Robberecht L, Delattre J, Meire M. 2023. Isthmus morphology influences debridement efficacy of activated irrigation: A laboratory study involving biofilm-mimicking hydrogel removal and high-speed imaging. Int Endod J. 56(1):118-127.
3. Brezhnev A, Tang FK, Kwan CS, Basabrain MS, Tsoi JKH, Matinlinna JP, *et al*. 2023. One-pot preparation of cetylpyridinium chloride-containing nanoparticles for biofilm eradication. ACS Appl Bio Mater. 6(3):1221-1230.
4. Mussagy CU, Santos-Ebinuma VC, Herculano RD, Coutinho JA, Pereira JF, Pessoa A. 2022. Ionic liquids or eutectic solvents?

Identifying the best solvents for the extraction of astaxanthin and β-carotene from *Phaffia rhodozyma* yeast and preparation of biodegradable films. Green Chem. 24(1):118-123.

5. Hu H, Kang X, Shan Z, Yang X, Bing W, Wu L, *et al*. 2022. A DNase-mimetic artificial enzyme for the eradication of drug-resistant bacterial biofilm infections. Nanoscale. 14(7):2676-2685.
6. Asare EO, Mun EA, Marsili E, Paunov VN. 2022. Nanotechnologies for control of pathogenic microbial biofilms. J Mater Chem B. 10(27):5129-5153.
7. Boominathan S, Suyambulingam I, Narayanaperumal S, Divakaran D, Senthamaraikannan P, Siengchin S. 2023. Comprehensive characterization of novel bioplasticizer from *Pandanus tectorius* leaves: A sustainable biomaterial for biofilm applications. Macromol Res. 31(11):1061-1075.
8. Cheng J, Zhang H, Lu K, Zou Y, Jia D, Yang H, *et al*. 2024. Bi-functional quercetin/copper nanoparticles integrating bactericidal and anti-quorum sensing properties for preventing the formation of biofilms. Biomater Sci. 12(7):1788-1800.
9. Zou L, Hu D, Wang F, Jin Q, Ji J. 2022. The relief of hypoxic microenvironment using an O_2 self-sufficient fluorinated nanoplatform for enhanced photodynamic eradication of bacterial biofilms. Nano Res. 15(2):1636-1644.
10. Zorzetto L, Scoppola E, Raguin E, Blank KG, Fratzl P, Bidan CM. 2023. Induced mineralization of hydroxyapatite in *Escherichia coli* biofilms and the potential role of bacterial alkaline phosphatase. Chem Mater. 35(7):2762-2772.
11. Mayorga-Martinez CC, Zelenka J, Klima K, Mayorga-Burrezo P, Hoang L, Ruml T, *et al*. 2022. Swarming magnetic photoactive microrobots for dental implant biofilm eradication. ACS Nano. 16(6):8694-8703.
12. Ronin D, Boyer J, Alban N, Natoli RM, Johnson A, Kjellerup BV. 2022. Current and novel diagnostics for orthopedic implant biofilm infections: A review. APMIS. 130(2):59-81.
13. Moradi M, Fazlyab M, Pourhajibagher M, Chiniforush N. 2022. Antimicrobial action of photodynamic therapy on *Enterococcus faecalis* biofilm using curing light, curcumin and riboflavin. Aust Endod J. 48(2):274-282.
14. Öztürk FY, Darcan C, Kariptaş E. 2023. The determination, monitoring, molecular mechanisms and formation of biofilm in *E. coli*. Braz J Microbiol. 54(1):259-277.
15. Dop RA, Neill DR, Hasell T. 2023. Sulfur-polymer nanoparticles: Preparation and antibacterial activity. ACS Appl Mater Interfaces. 15(17):20822-20832.
16. Cui Y, Wang D, Zhang L, Qu X. 2025. Research progress on the regulatory mechanism of biofilm formation in probiotic lactic acid bacteria. Crit Rev Food Sci Nutr. 65(25):4869-4883.
17. Wang J, Jiang Z, Wei Y, Wang W, Wang F, Yang Y, *et al*. 2022. Multiplexed identification of bacterial biofilm infections based on machine-learning-aided lanthanide encoding. ACS Nano. 16(2):3300-3310.
18. Erum N, Ahmad J. 2024. Structural, elastic and mechanical properties of cubic perovskite materials. Arch Adv Eng Sci. 2(1):24-29.